Catalysis
Science & Technology

RSC Publishing

PAPER

View Article Online
View Journal | View Issue

Cite this: *Catal. Sci. Technol.*, 2013, **3**, 1063

Effect of tetrahedral aluminum on the catalytic performance of Al–SBA-15 supported Ru catalysts in Fischer–Tropsch synthesis

Sufang Chen,[ab] Jinlin Li,*[c] Yuhua Zhang,[ac] Yanxi Zhao[ac] and Jinping Hong[c]

Received 22nd October 2012,
Accepted 14th December 2012

DOI: 10.1039/c2cy20716h

www.rsc.org/catalysis

Al–SBA-15 supports were synthesized by both direct synthesis and post-synthesis grafting methods. The two synthetic methods lead to different tetrahedral Al sites; Al(*x*)-D samples prepared by direct synthesis exhibit more tetrahedral Al sites than Al(*x*)-P supports prepared by the post-synthesis grafting method as determined by ^{27}Al magic-angle-spinning NMR (^{27}Al MAS NMR). The temperature-programmed desorption of ammonia (NH_3-TPD) result shows that the material with more tetrahedral Al sites has higher acidity. The Al–SBA-15 material supported ruthenium catalysts were applied in Fischer–Tropsch synthesis (FTS). The tetrahedral Al content is shown to promote the dispersion of ruthenium in the supported catalysts, which is illustrated by powder X-ray diffraction (XRD), nitrogen adsorption–desorption and hydrogen temperature programmed desorption (H_2-TPD). The effect of tetrahedral Al on the catalytic selectivity was discussed. The selectivity of long chain hydrocarbons (C_{11+}) is lower for the catalyst with higher content of tetrahedral Al sites in FTS.

1. Introduction

Fischer–Tropsch synthesis (FTS) is a heterogeneous catalytic process for the production of hydrocarbons from syngas ($CO + H_2$). Many supported metal catalysts are used in Fischer–Tropsch synthesis, such as Co, Fe and Ru based catalysts.[1] Despite the higher price of Ru as compared with Co and Fe, Ru-based catalysts are suitable for fundamental research to obtain clear-cut information about the effect of the supports since Ru precursors can be easily reduced to Ru^0 and the size of Ru^0 particles can be controlled facilely over different supports.[2] The development of catalysts with high selectivity to a specific range of products is still one of the most important challenges in FTS. It is well known that the support acidity leads to a change in selectivity. The combination of acid catalysts, typically aluminosilicates (*e.g.* zeolites), with a conventional FTS catalyst to form a bifunctional catalyst system may increase the product selectivity to a specific range.[2–5] The catalytic activity of acidic aluminosilicates is usually assumed to reside in sites involving tetrahedral aluminum atoms at substitutional positions in the framework of silica.[6] Paul B. Weisz[7] clearly demonstrated that tetrahedral aluminum sites in the silica structure provided more ''active sites''. Wei *et al.*[8] studied FTS over Co–Ir catalysts supported on mesoporous aluminosilicate (MPAS), and found that CO conversion and selectivity for C_{10}–C_{20} hydrocarbon products were increased and selectivity for CH_4 was effectively restrained. The beneficial effect was attributed to tetrahedral aluminum sites.

Compared to conventional zeolites generally with micropores, the ordered mesoporous aluminosilicates Al–SBA-15 with higher surface area and larger pore volume have attracted increasing attention recently.[9] With the presence of weak acid sites in Al–SBA-15, the product selectivity could be regulated.[4,10] Kim *et al.*[4] reported that Fe-based FTS catalysts supported on Al–SBA-15 exhibited the maximum diesel fuel fraction (C_{11+} hydrocarbons) with an Al/Si ratio of 0.010. Ooi *et al.*[10] found that the Al–SBA-15 catalyst was more selective towards the gasoline fraction in the liquid products as compared to SBA-15 in catalytic cracking of a waste palm oil based fatty acid mixture.

The aim of this work is to study the influence of tetrahedral Al sites on the product selectivity in FTS over Al–SBA-15 supported Ru catalysts. Two methods, direct synthesis and post-synthesis grafting, have been developed in order to introduce tetrahedral aluminum into the framework of mesoporous

[a] *College of Chemistry, Chemical Engineering and Materials Science, Soochow University, Suzhou, Jiangsu 215006, China. E-mail: csfzdh@126.com*
[b] *Key Laboratory for Green Chemical Process of Ministry of Education, School of Chemical Engineering and Pharmacy, Wuhan Institute of Technology, Wuhan, Hubei 430073, China*
[c] *Key Laboratory of Catalysis and Materials Science of the State Ethnic Affairs Commission & Ministry of Education, South-Central University for Nationalities, Wuhan, Hubei 430073, China. E-mail: jinlinli@yahoo.cn; Fax: +86 27 67842752; Tel: +86 27 67843016*

silica materials. The correlation between tetrahedral Al sites of the catalyst and product selectivity in FTS has been analyzed and discussed in detail.

2. Experimental section

2.1. Preparation

Support preparation. SBA-15 material was obtained using Pluronic P123 ($(EO_{20}PO_{70}EO_{20}$, MAV) 5800, BASF) and tetraethyl orthosilicate (TEOS, AR) under acidic conditions following the method reported in the literature.[11] Its detailed synthetic route is as follows: P123 (10 g) was dissolved in a solution of 2 M HCl (350 ml) under stirring at 313 K. Subsequently, TEOS (21 g) was gradually added. The mixture was continuously stirred for 48 h and then transferred into a closed Teflon bottle and kept at 373 K for 48 h. The precipitated material was then filtered, washed with deionized water, dried at 383 K overnight and calcined at 823 K for 6 h (1 K min^{-1}).

Al–SBA-15 materials prepared by the direct synthesis method according to the literature[12] are denoted Al(x)-D. Typically, Al–SBA-15 materials were prepared by the following process: P123 (4 g) and HCl (150 ml, pH = 1.5) were mixed and stirred at 313 K to obtain a transparent solution, then NH_4F (0.05 g) was added and dissolved completely, and the solution was marked A. Afterwards, TEOS (9 ml) and a certain amount of aluminum isopropoxide were added to a solution of HCl (10 ml, pH = 1.5) to obtain solution B. Solution B was stirred at 313 K for 3 h, and then added dropwise into solution A. The obtained mixture was stirred for 20 h at 313 K, and then transferred into a closed Teflon bottle and kept at 373 K for 48 h. Finally, the product was filtered, washed with deionized water, dried at 383 K overnight and calcined at 823 K for 6 h (1 K min^{-1}) in air.

Al–SBA-15 prepared by post-synthetic grafting is denoted Al(x)-P, using the same procedure in the literature.[13] Particularly, calcined pure siliceous SBA-15 (2 g) was dispersed in hexane (100 ml), and then a small amount of hexane containing different amounts of aluminum isopropoxide was added under stirring. The resulting mixture was stirred at room temperature for another 24 h. The products were filtered, washed with hexane repeatedly, dried overnight at 373 K in air, and further calcined at 823 K (heating rate 1 K min^{-1}) for 4 h. The x, D and P in the Al-containing SBA-15 samples Al(x)-D and Al(x)-P correspond to the Al/Si molar ratio in the product determined by ICP-AES, direct synthesis and post-synthesis grafting respectively.

Catalyst synthesis. The Ru (4 wt%)-based catalysts were prepared by the "two solvent technique" reported in the literature.[14] In a typical synthesis process, 1 g of support was dispersed in 40 ml of dry *n*-hexane (as one solvent). After stirring for 3 h, a small amount of water (another solvent, the amount was equal to the porous volume of the support) containing the required amount of $Ru(NO)(NO_3)_3$ was added dropwise. The solution was continuously stirred for 12 h at room temperature, and then dried at 373 K for 10 h in air. The catalysts were denoted 4Ru(x)-D and 4Ru(x)-P, corresponding to Al(x)-D and Al(x)-P supported ruthenium catalysts, respectively. The 4Ru(0) catalyst corresponds to the pure SBA-15 supported ruthenium catalyst.

In addition, another catalyst supported on Al(0.033)-D with the same Ru loading of 4 wt% was prepared by the incipient wetness impregnation method. This catalyst was dried at 373 K for 10 h and denoted 4Ru(0.033)-DI.

2.2. Characterization

The chemical compositions of all the materials were determined by inductive coupled plasma-atomic emission spectroscopy (ICP-AES) on a Varian Vista AX CD system.

The nitrogen adsorption–desorption experiment was conducted at 77 K with a Quantachrome Autosorb-1-C-MS. Before measurement, the samples were outgassed at 473 K for 6 h. The surface area was obtained using the Brunauer–Emmett–Teller (BET) model for adsorption with the relative pressure ranging from 0.05 to 0.30. The pore volumes were calculated from the amount of N_2 vapor adsorbed at a relative pressure of 0.99, assuming that the pores were filled with the condensate in the liquid state. The pore size distribution was evaluated from the desorption branches of the isotherms using the Barrett–Joyner–Halenda (BJH) method.

The X-ray diffraction (XRD) patterns were obtained by using a Bruker-D8 powder X-ray diffractometer equipped with monochromatized Cu-Kα radiation (λ = 1.54056 Å) and a VANTEC-1 detector, and operating at 40 kV and 40 mA.

^{27}Al magic-angle-spinning NMR (^{27}Al MAS NMR) for all the samples were performed at room temperature with a 4.0 mm MAS probe on a Bruker Advance III-400 spectrometer with a magnetic field strength of 9.4 T at a frequency of 104.2 MHz. The powder sample was packed inside zirconia MAS rotors and spun at 14 kHz. The ^{27}Al MAS spectrum was obtained using a single hard pulse, with radiofrequency powers of 83 kHz. ^{27}Al chemical shifts were set at 0 ppm referencing to $Al(NO_3)_3{\cdot}9H_2O$.

The temperature-programmed desorption of ammonia (NH_3-TPD) was conducted on a Micromeritics AutoChem 2920II instrument. Typically, 0.05 g of the dried sample was loaded into a U-shaped quartz tube and pretreated in a helium flow at 773 K for 2 h. Then, the sample was cooled down to 353 K and saturated with NH_3 gas for 0.5 h. The sample was flushed with helium flow for 1 h to remove the gas phase and the physically adsorbed NH_3-TPD profile of ammonia recorded from 353 K to 1023 K with a ramping rate of 10 K min^{-1}. The process of desorption was monitored by an online quadruple mass spectrometer (HIHEN QIC-20) equipped with a heated capillary interface. A mass number of 16 was followed to obtain the TPD profiles of NH_3 because the mass intensity was relatively strong, and the interferences from H_2O were negligible.[15]

The dispersion degree and size of the Ru particles were calculated from hydrogen temperature programmed desorption (H_2-TPD) data measured on a Zeton Altamira AMI-200 unit. The sample weight was about 0.05 g. The catalyst was reduced at 623 K for 12 h using a flow of high purity hydrogen and then cooled to 373 K under hydrogen stream. The sample was held at 373 K for 1 h under flowing argon to remove weakly bound physisorbed species prior to increasing the temperature slowly to 623 K. At this temperature, the catalyst was held under flowing

argon to desorb the remaining chemisorbed hydrogen, and the TCD began to record the signal until the signal returned to the baseline. The TPD spectrum was integrated and the amount of desorbed hydrogen was determined by comparing the mean areas of calibrated hydrogen pulses. Prior to the experiments, the sample loop was calibrated with pulses of nitrogen in helium flow, compared with the signal produced from a gas tight syringe injection (100 μL) of nitrogen under helium flow. The formula for the calculation of the dispersion degree and cluster size were reported in previous studies.[16]

2.3. Fischer–Tropsch synthesis (FTS)

FTS reaction was conducted in a fixed bed reactor (id = 12 mm) at 503 K and 1.0 MPa. The catalyst (0.4 g) was mixed with 4.0 g carborundum and reduced in a flow of high purity H_2 with a space velocity of 3 N L h^{-1} g^{-1} (298 K, 0.1 MPa). The reactor temperature was increased from ambient to 373 K with 2 K min^{-1}, followed by increasing to 623 K at 1 K min^{-1} and held for 10 h at 673 K. After reduction, the catalyst was cooled to 373 K in flowing H_2. Then, the syngas (H_2/CO = 2) was introduced and the pressure was increased to 1.0 MPa. The reactor temperature was then slowly increased to 503 K with 1 K min^{-1}, and the space velocity of syngas was 4 S L h^{-1} g^{-1} (273 K, 0.1 MPa). The wax and water products were collected in a hot trap (373 K), and the oil and water products were collected in a cold trap (271 K). The outlet gas was analyzed online using an Agilent 3000A Micro GC. The oil and wax products were analyzed with an Agilent 6890N GC and an Agilent 7890A GC, respectively.

3. Results and discussion

3.1. Characterization of catalysts and supports

The Al/Si ratio of the supports determined by ICP-AES is shown in Table 1. When the Al/Si ratio was applied in the synthesis gel, a much lower Al/Si ratio was obtained in the product for the Al(x)-D supports, while a slightly higher ratio was detected for the Al(x)-P support. A similar finding has been observed in the previous literature.[17] The lower Al/Si ratio for Al(x)-D supports can be attributed to the partial loss of the extra framework aluminum during washing in the direct-synthesis method.[18] All the catalysts have a similar Ru content (around 4 wt%) as shown in Table 1, indicating no loss of Ru during preparation of the catalysts.

Textural properties calculated by the N_2 adsorption isotherm are listed in Table 1. The data for the SBA-15 show high surface area (634.9 m^2 g^{-1}) and pore volume (1.31 cm^3 g^{-1}), which are changed by Al incorporation. A remarkable increase in the surface area and pore volume as compared to those of the pure SBA-15 is noted when aluminum was introduced by the direct synthesis method, contributed by the development of micropores and secondary mesopores.[17] However, the surface area and pore volume of support are decreased significantly when Al was incorporated by the post-synthesis grafting method, attributable to a slight distortion of the mesoporous channels from the deposition of Al clusters on the inner pore walls of the SBA-15.[19] This trend is in good agreement with the results reported by Dragoi *et al.*[17] After the loading of ruthenium, the surface area and total pore volume of the catalysts decrease to some extent, suggesting that most of the Ru particles are uniformly loaded inside the channels, leading to the reduction of the surface area and pore volume.

N_2 adsorption–desorption isotherms of the supports and catalysts are shown in Fig. 1a and b. All the isotherms indicate the preservation of the SBA-15 structure with 2D-hexagonal structure.[20] The BJH pore diameters of supports are shown in Fig. 1c. The pore diameters of both pure SBA-15 and Al(x)-D samples are centered at around 7.4 nm, indicating that Al^{3+}

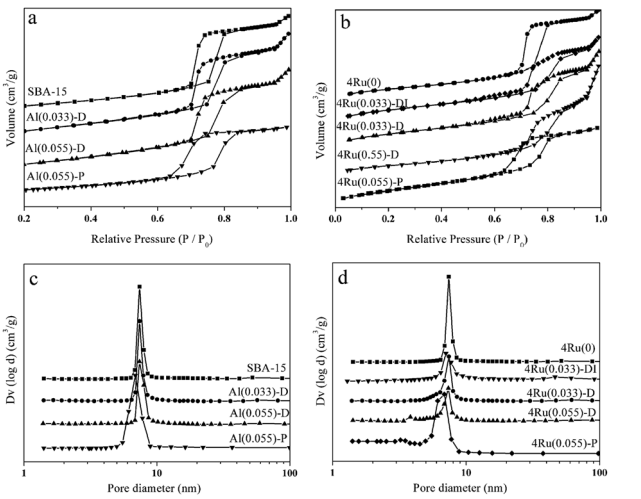

Fig. 1 N_2 adsorption–desorption isotherms of (a) supports; (b) catalysts and BJH pore size distribution curves of (c) supports; (d) catalysts.

Table 1 Textural parameters of mesoporous samples

Supports	Al/Si ratio: In the gel	Al/Si ratio: In the product[a]	S_{BET}[b] (cm^2 g^{-1})	V_{Total}[c] (cm^3 g^{-1})	d_{BJH}[d] (nm)	Catalysts	Ru[a] (wt%)	S_{BET}[b] (cm^2 g^{-1})	V_{Total}[c] (cm^3 g^{-1})	d_{BJH}[d] (nm)
SBA-15	0	0	634.9	1.31	7.4	4Ru(0)	3.99	540.8	1.24	7.4
Al(0.033)-D	0.05	0.033	700.3	1.52	7.4	4Ru(0.033)-DI	3.98	649.6	1.21	7.0
						4Ru(0.033)-D	4.00	667.3	1.33	7.4
Al(0.055)-D	0.10	0.055	603.2	1.72	7.4	4Ru(0.055)-D	4.00	472.6	1.46	7.4
Al(0.055)-P	0.05	0.055	471.3	1.05	6.8	4Ru(0.055)-P	3.97	385.4	0.82	6.8

[a] Al/Si ratio in the product calculated from ICP-AES. [b] BET specific surface area. [c] Total pore volume. [d] Pore diameter calculated by the BJH method.

does not induce pore blocking.[21] However, for the Al(0.055)-P sample, the pore diameter is centered at around 6.8 nm, which might be caused by a slight distortion of the mesoporous channels or pore narrowing due to the deposition of Al clusters on the inner pore walls.[17] The BJH pore diameters of Ru catalysts are shown in Fig. 1d. Compared with the corresponding supports, the pore diameter of the catalysts prepared by the "two-solvent technique" is essentially unchanged, while the pore diameter of the 4Ru(0.033)-DI catalyst prepared by the incipient wetness impregnation method is decreased, indicating that a portion of the channels in the support is blocked by Ru nanoparticles in the catalyst prepared by the incipient wetness impregnation method.

Small-angle XRD patterns (Fig. 2a) of all the supports exhibit three well-resolved diffraction peaks, indexed to the (100), (110) and (200) reflections of the hexagonal space group *p6mm*,[11] which suggests the preservation of the SBA-15 structure after incorporation of Al either by direct synthesis or post-synthesis grafting, consistent with the results of N_2 adsorption–desorption isotherms. Fig. 2b shows the larger-angle powder XRD patterns of Ru-based catalysts after reduction at 573 K for 3 h in a tube furnace (2 K min^{-1}) under hydrogen. The very broad diffraction peak at a 2θ of around 25° is typical reflection of amorphous silica.[22] The diffraction peak assigned to metallic Ru (JCPDS 00-006-0663) at a 2θ of around 44° is observed for all supported catalysts.[21]

^{27}Al MAS NMR spectra of the supports are shown in Fig. 3. The peak at δ 53 ppm is ascribed to the framework aluminum species in tetrahedral coordination (Al_{tetra}), while the peak at δ 0 ppm is assigned to extra-framework aluminum species in octahedral coordination (Al_{octa}).[23] Fig. 3b shows the distribution of Al sites, which is calculated by the method reported by Boissière *et al.*[24] For the Al(0.033)-D and Al(0.055)-D samples, the proportion of Al_{tetra}/Al_{octa} has a global tendency to decrease with increasing Al/Si ratio in the product, indicating that the proportion of extra-framework aluminum sites increases as well. Compared with Al(0.055)-D and Al(0.055)-P, which have the same Al/Si ratio in the final product, the ratio of Al_{tetra}/Al_{octa} in Al(0.055)-D is higher than that in Al(0.055)-P, indicating that the direct synthetic method can produce more framework aluminum sites than the post-synthesis grafting.

NH_3-TPD profiles of supports are shown in Fig. 4. All the supports exhibit a desorption peak at 353–473 K, which relates to the desorption of physically adsorbed NH_3.[25] Other desorption peaks of NH_3 in the range of 450 K to 850 K are observed only for Al containing SBA-15 supports, indicating the presence of different

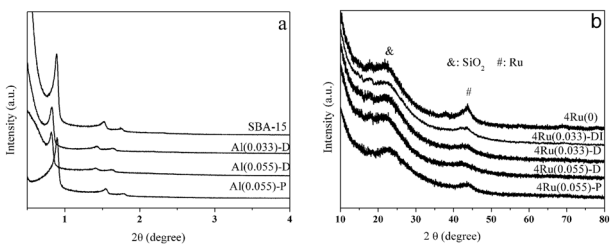

Fig. 2 (a) Small-angle XRD patterns of supports; (b) large-angle XRD patterns of catalysts.

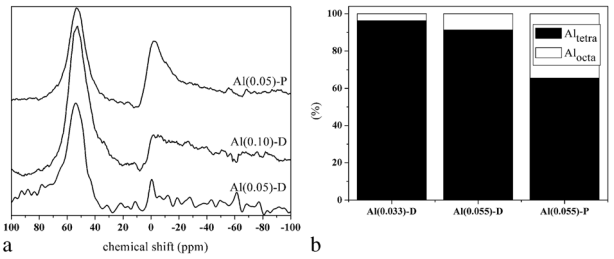

Fig. 3 (a) ^{27}Al MAS-NMR spectra of Al(*x*)-SBA-15; (b) distribution of Al sites.

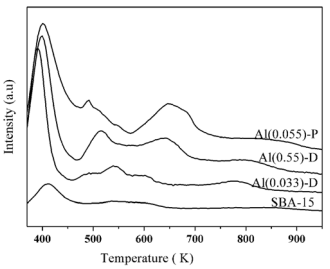

Fig. 4 NH_3-TPD profiles of the supports.

types of acid sites. The peaks located at the lower desorption temperature range of 450 K to 570 K can be attributed to tetrahedral coordinated aluminum which has weak acidity whereas the peaks at the higher desorption temperature range (570–850 K) are ascribed to octahedral coordinated Al with stronger acidity.[26] It is interesting to note that with increasing Al content, the desorption temperature of ammonia is significantly increased.

Table 2 shows the content of tetrahedral aluminum (Al_{tetra}) in the supports determined by ICP-AES and ^{27}Al MAS NMR. Comparing 4Ru(0.055)-D with 4Ru(0.055)-P at the same Al/Si ratio, the Al_{tetra} content in Al(0.055)-D and in Al(0.055)-P samples are 5.11% and 3.62%, respectively, indicating that the content of Al sites differ from those obtained by synthetic methods of supports. Table 2 also lists the results of hydrogen temperature-programmed desorption (H_2-TPD) of the catalysts. On the one hand, the dispersion degree is related to the catalyst preparation methods. Comparing 4Ru(0.033)-D with 4Ru(0.033)-DI catalysts supported on the same Al(0.033)-D support, the dispersion degree of Ru in the 4Ru(0.033)-D catalyst prepared by the "two solvent technique" is 69.5%, while that in the 4Ru(0.033)-DI catalyst prepared by the incipient wetness impregnation method is 48.1%, indicating that the "two solvent technique" could improve the dispersion of active metals. On the other hand, when these catalysts (4Ru(0), 4Ru(0.033)-D, 4Ru(0.055)-D and 4Ru(0.055)-P) are prepared by the same "two solvent technique", the dispersion degree is related to the Al_{tetra} content. Initially, the dispersion degree of Ru increases remarkably with increasing Al_{tetra} content, and then changes slowly with a further increase in Al_{tetra} content.

3.2. Catalytic performance in FTS

Catalytic activity. The FTS activity, measured as CO conversion at 503 K under 80 hours' reaction in the quasi-steady state, is presented in Table 2. As shown, Ru species on the low

Table 2 The activity and selectivity of hydrocarbons in FTS

Samples	Al_{tetra}[a] (%)	Dispersion[b] (%)	D_{Ru}[b] (nm)	CO[c] (%)	CH_4 (%)	C_2–C_4 (%)	C_5–C_{10} (%)	C_{11+} (%)
4Ru(0)	0	24.2	6.4	22.2	23.9	13.6	20.6	41.9
4Ru(0.033)-DI	3.17	48.1	3.2	28.7	24.8	17.5	26.7	31.0
4Ru(0.033)-D	3.17	69.5	2.2	25.3	25.7	17.8	25.7	30.8
4Ru(0.055)-P	3.62	73.3	2.1	19.5	26.2	20.0	31.1	22.7
4Ru(0.055)-D	5.11	86.1	1.8	14.2	27.6	27.0	35.2	10.2

[a] Al_{tetra} in the product (%) = (Al/Si ratio in product) × $Al_{tetra}/(Al_{tetra} + Al_{tetra})$ × 100%. [b] Calculated from H_2-TPD. [c] Reaction conditions: 1.0 MPa, 503 K, H_2/CO = 2, 4 S L h^{-1} g^{-1}, FTS data were collected at the steady state (80 h).

aluminum-content Al–SBA-15 supports are more active than those on the high aluminum-content ones. The decrease in the catalytic activity should be attributed to the too high dispersion of Ru. Kellner and Bell[27] reported that the decrease in catalytic activity with increasing Ru dispersion from 30% to 70% was attributed to a decrease in the content of active sites locating on planar surfaces of the Ru microcrystallites. The much faster decrease in catalytic activity, observed at a dispersion greater than 70%, was due to changes in the electronic properties of the very small crystallites and the interaction between the crystallites and the support.

Catalyst selectivity. Table 2 also lists the product selectivity of the catalysts in FTS. The selectivity of the long chain hydrocarbon fraction (C_{11+}) decreases while that of the short chain hydrocarbon ($<C_{11+}$) increases with increasing Al_{tetra} content. To illustrate the effect of the Al_{tetra} content on the selectivity of hydrocarbons in FTS, the following three aspects are discussed. Firstly, the selectivities of hydrocarbons are compared between the 4Ru(0.033)-DI catalyst and the 4Ru(0.033)-D catalyst, which have the same Al_{tetra} content but different Ru particle size. As shown in Table 2, the product selectivities of these two catalysts are basically the same in all ranges, suggesting that selectivity of hydrocarbons is faintly affected by Ru particle size within a certain range. Similar results were reported by Carballo *et al.*[28] on Ru/γ-Al_2O_3. Secondly, the selectivities of hydrocarbons for the three catalysts (4Ru(0.033)-D, 4Ru(0.055)-D and 4Ru(0.055)-P), with a similar Ru particle size but different Al_{tetra} content, are compared. The results show that the catalyst with a higher Al_{tetra} content exhibits lower selectivity of C_{11+} hydrocarbons. The above two aspects confirm that the product selectivity is affected not by Ru particle size within a certain range but mainly by the Al_{tetra} content. Finally, the selectivities of hydrocarbons for the two catalysts (4Ru(0.055)-P and 4Ru(0.055)-D) in possession of the same Al/Si ratio but different Al_{tetra} content are compared. The 4Ru(0.055)-D catalyst with a higher Al_{tetra} content exhibits lower selectivity for C_{11+} hydrocarbons. This also confirms that the product selectivity is mainly dependent on the Al_{tetra} content rather than on the Al/Si ratio. Combined with the findings by Secundo *et al.*,[29] the tetrahedral coordinated Al is an acid active site, and the tetrahedral coordination Al active site plays an important role in the selectivity of C_{11+} hydrocarbons in FTS.

4. Conclusion

Mesoporous aluminosilicates Al–SBA-15 with different Al_{tetra} contents were synthesized by both direct synthesis and post-synthesis grafting methods, and the corresponding Ru-based catalysts were used in FTS. The catalytic performance is strongly dependent on the Al_{tetra} content of the support. The Ru dispersion degree of the catalyst increases with increasing Al_{tetra} content. The results of catalytic tests in FTS show that the activity is mainly affected by the dispersion degree. The product selectivity is mainly determined by the Al_{tetra} content rather than by the Al/Si ratio or Ru particle size within a certain range. The higher Al_{tetra} content in the catalyst corresponds to lower selectivity of long chain hydrocarbons (C_{11+}) in FTS.

Acknowledgements

This work was supported by National Natural Science foundation of China (21073238 and 21203255), National Basic Research Program of China (2011CB211704), and the Special Fund for Basic Scientific Research of Central Colleges, South-Central University for Nationalities.

Notes and references

1 Q. H. Zhang, J. C. Kang and Y. Wang, *ChemCatChem*, 2010, **2**, 1030–1058.
2 K. Cheng, J. C. Kang, S. W. Huang, Z. Y. You, Q. H. Zhang, J. S. Ding, W. Q. Hua, Y. C. Lou, W. P. Deng and Y. Wang, *ACS Catal.*, 2012, **2**, 441–449.
3 Y. Li, T. Wang, C. Wu, X. Qin and N. Tsubaki, *Catal. Commun.*, 2009, **10**, 1868–1874.
4 D. J. Kim, B. C. Dunn, F. Huggins, G. P. Huffman, M. Kang, J. E. Yie and E. M. Eyring, *Energy Fuels*, 2006, **20**, 2608–2611.
5 A. Martínez, C. Lopéz, E. Peris and A. Corma, *Stud. Surf. Sci. Catal.*, 2005, **158**, 1327–1334.
6 W. Haag, R. Lago and P. Weisz, *Nature*, 1984, **309**, 589–591.
7 P. B. Weisz, *Ind. Eng. Chem. Fundam.*, 1986, **25**, 53–58.
8 M. Wei, K. Okabe, H. Arakawa and Y. Teraoka, *New J. Chem.*, 2002, **26**, 20–23.
9 F. S. Xiao, *Top. Catal.*, 2005, **35**, 9–24.
10 Y. S. Ooi, R. Zakaria, A. R. Mohamed and S. Bhatia, *Catal. Commun.*, 2004, **5**, 441–445.
11 D. Y. Zhao, J. L. Feng, Q. S. Huo, N. Melosh, G. H. Fredrickson, B. F. Chmelka and G. D. Stucky, *Science*, 1998, **279**, 548–552.
12 Y. Li, Q. H. Yang, J. Yang and C. Li, *J. Porous Mater.*, 2006, **13**, 187–193.
13 J. M. R. Gallo, C. Bisio, G. Gatti, L. Marchese and H. O. Pastore, *Langmuir*, 2010, **26**, 5791–5800.

14 I. Lopes, N. El Hassan, H. Guerba, G. Wallez and A. Davidson, *Chem. Mater.*, 2006, **18**, 5826–5828.
15 Z. T. Zhang, Y. Han, L. Zhu, R. W. Wang, Y. Yu, S. L. Qiu, D. Y. Zhao and F. S. Xiao, *Angew. Chem., Int. Ed.*, 2001, **40**, 1258–1262.
16 J. Okal, M. Zawadzki, L. Kępiński, L. Krajczyk and W. Tylus, *Appl. Catal., A*, 2007, **319**, 202–209.
17 B. Dragoi, E. Dumitriu, C. Guimon and A. Auroux, *Microporous Mesoporous Mater.*, 2009, **121**, 7–17.
18 J. Ma, L. S. Qiang, J. F. Wang, X. B. Tang and D. Y. Tang, *J. Porous Mater.*, 2011, **18**, 607–614.
19 S. J. Wu, J. H. Huang, T. H. Wu, K. Song, H. S. Wang, L. H. Xing, H. Y. Xu, L. Xu, J. Q. Guan and Q. B. Kan, *Chin. J. Catal.*, 2006, **27**, 9–14.
20 A. Taguchi and F. Schüth, *Microporous Mesoporous Mater.*, 2005, **77**, 1–45.
21 H. F. Xiong, Y. H. Zhang, S. G. Wang, K. Y. Liew and J. L. Li, *J. Phys. Chem. C*, 2008, **112**, 9706–9709.
22 J. Ma, L. S. Qiang, J. F. Wang, D. Y. Tang and X. B. Tang, *Catal. Lett.*, 2010, **141**, 1–8.
23 M. Gómez-Cazalilla, J. M. Mérida-Robles, A. Gurbani, E. Rodríguez-Castellón and A. Jiménez-López, *J. Solid State Chem.*, 2007, **180**, 1130–1140.
24 C. Boissière, L. Nicole, C. Gervais, F. Babonneau, M. Antonietti, H. Amenitsch, C. Sanchez and D. Grosso, *Chem. Mater.*, 2006, **18**, 5238–5243.
25 T. Klimova, L. Lizama, J. C. Amezcua, P. Roquero, E. Terrés, J. Navarrete and J. M. Domínguez, *Catal. Today*, 2004, **98**, 141–150.
26 P. Srinivasu, S. Alam, V. V. Balasubramanian, S. Velmathi, D. P. Sawant, W. Böhlmann, S. P. Mirajkar, K. Ariga, S. B. Halligudi and A. Vinu, *Adv. Funct. Mater.*, 2008, **18**, 640–651.
27 C. S. Kellner and A. T. Bell, *J. Catal.*, 1982, **75**, 251–261.
28 J. M. G. Carballo, J. Yang, A. Holmen, S. García-Rodríguez, S. Rojas, M. Ojeda and J. L. G. Fierro, *J. Catal.*, 2011, **284**, 102–108.
29 F. Secundo, G. Roda, M. Vittorini, A. Ungureanu, B. Dragoi and E. Dumitriu, *J. Mater. Chem.*, 2011, **21**, 15619–15628.

